SIMULTANEOUS DENSITY AND VELOCITY MEASUREMENT FOR ROTORCRAFT RESEARCH IN A TRANSONIC WIND TUNNEL

H.Richard*,W.Geissler**,M.Raffel*

Deutsches Zentrum für Luft- und Raumfahrt e.V. (DLR)

Institut für Strömungsmechanik,Göttingen,Germany

Abstract:

The present paper describes two different experiments performed in a transonic wind tunnel facility at DLR-Göttingen. The first experiment was conducted in order to study compressible vortices behind a cylinder and investigating the feasibility of combining two different measuring techniques: the Background Oriented Schlieren (BOS) technique and the Particle Image Velocimetry (PIV) which allow respectively to measure both density and velocity fields.

The second experiment described in the present paper is done in the same wind tunnel facility where a new test section has been developed to investigate the unsteady flow about oscillating models under dynamic stall conditions. Dynamic stall is characterized by the development, movement and shedding of one or more concentrated vortices on the blade upper surface. The hysteresis loops of lift-, drag- and pitching moment are highly influenced by these vortices. To understand the very complicated unsteady flow involved, a detailed knowledge of the instantaneous flow fields is of crucial importance. With the application of the described measuring techniques it is expected to gain more insight into the problem.

In recent years numerical codes based on the time-accurate solution of the Reynolds-Averaged Navier-Stokes equations (RANS) have been developed. Results from these codes are ready for comparison with experimental data. A section of the present paper is dedicated to the comparison of numerical with corresponding experimental data.

1.Introduction

In recent years the dynamic stall problem on helicopter rotor blades gained considerable interest in both Europe and the US. The dynamic stall problem has been investigated for a long time; a large number of papers and publications exist on this subject (see i.e. [1],[2]). However the complexity of the flow is high and the problem is still not completely understood. Dynamic stall limits the flight envelope of the helicopter.

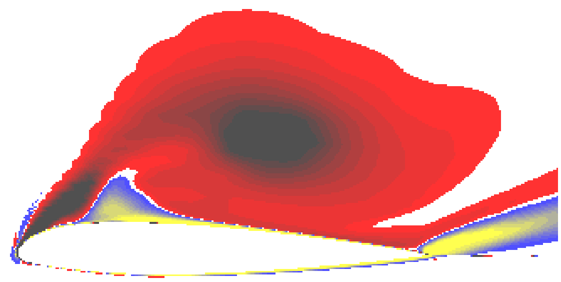

Fig.1: Dynamic stall vortex development

It is therefore of high interest to **influence** dynamic stall in such a way that high drag and negative pitching moment peaks are avoided without loosing lift. For the consequent development of reliable dynamic stall control technologies (see [3]) it is inevitable to be able to understand the complex flows involved.

Two of the most important features of the dynamic stall process are displayed in Figs.1 and 2. Fig.1 shows calculated vorticity contours [4] at about 19^o upstroke of a NACA 23012 airfoil under deep dynamic stall conditions. A strong vortex is developing and moving along the airfoil upper surface. Only a short time later this vortex lifts off the surface and is shedded into the

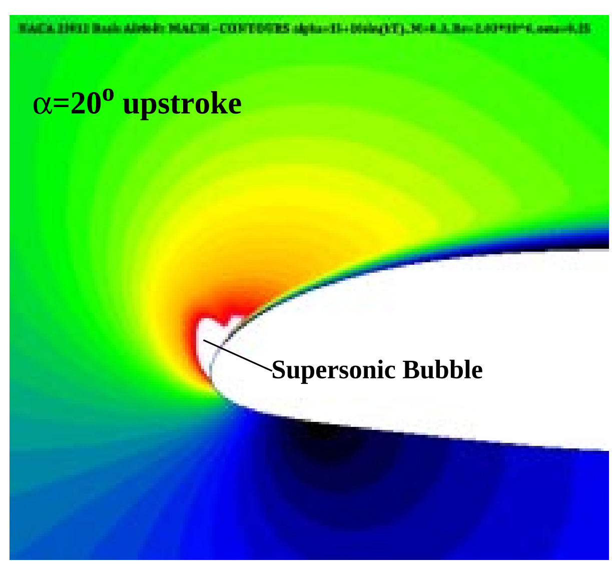

Fig.2: Compressibility effect on NACA23012 airfoil

* Research Scientist

** Senior Research Scientist

wake. A counter rotating vortex is developing at the airfoil trailing edge. These events have a strong impact on lift-, drag- and pitching moment: When the vortex leaves the airfoil the drag is increasing and the pitching moment shows a strong negative peak. At the same time the lift which has reached a considerable higher level compared to the steady case breaks down immediately. Strong hysteresis effects occur during the down stroke part of the airfoil motion.
A second important effect is shown in Fig.2. This figure displays calculated Mach contours around the airfoil leading edge. The white spot at the airfoil leading edge indicates that the flow in this very limited area is supersonic although the main flow has a low Mach number of M=0.3. The supersonic bubbles are terminated by very short but strong shock waves. These effects have also been measured (see i.e.[5]). It is assumed that the compressibility effects serve as a trigger of the dynamic stall process.
Due to these observations of dynamic stall vortices with strong vorticity contents and compressibility effects triggering the dynamic stall process it is very obvious that new suitable measuring techniques are necessary to look into the details of these different flow phenomena.
The PIV technique [6] gives the opportunity to measure instantaneous velocity fields from which the vorticity distribution can directly be derived. The BOS technique [7] is able to measure the instantaneous density fields about a moving model. The combination of both techniques in simultaneous mode may give the still missing parts of the dynamic stall problem.
The following discussion is split into three different parts:
Part 1: Description of combined PIV and BOS experiment for the flow about a circular cylinder.
Part 2: Description of the dynamic stall experiment on oscillating airfoils under deep dynamic stall conditions.
Part 3: Discussion of results of the dynamic stall experiments and comparisons with numerical data.

2. Combined PIV and BOS Experiment for Flow about a Circular Cylinder (Part 1).

The experiment described was setup in order to study compressible vortex flows related to the BVI-phenomenon of helicopter rotors in more detail. Therefore, the vortex shedding on a cylinder with a diameter of 25 mm has been investigated in a transonic wind tunnel by simultaneous velocity and density gradient measurements at different free stream Mach numbers. This information was complemented by additional measurements of the unsteady pressure fluctuations at different locations along the wind tunnel walls. This data enables a more detailed analysis of compressible vortices than successive measurements of single quantities, because they require certain assumptions to be made in order to describe the gas dynamics of compressible vortices. However, a detailed description of compressible vortices plays a key role in numerical simulations, which are aimed by many research organizations for a further improved prediction of helicopter noise. The measurement of the velocity induced by the vortex is needed, since the amplitude of the pressure waves, which are emitted during the interaction of the vortex with a blade, is proportional to the circulation of the vortex. In the past the velocity information has been derived by simultaneous pressure and density measurements (e.g. Mandella and Bershader 1987). Therefore it had to be assumed that the vortex is moving with constant convection speed, that it is symmetrical with respect to it's axis, and that the vortex can be described by a solution of the stationary Euler-equations, which means that the vortex moves without a signifi-

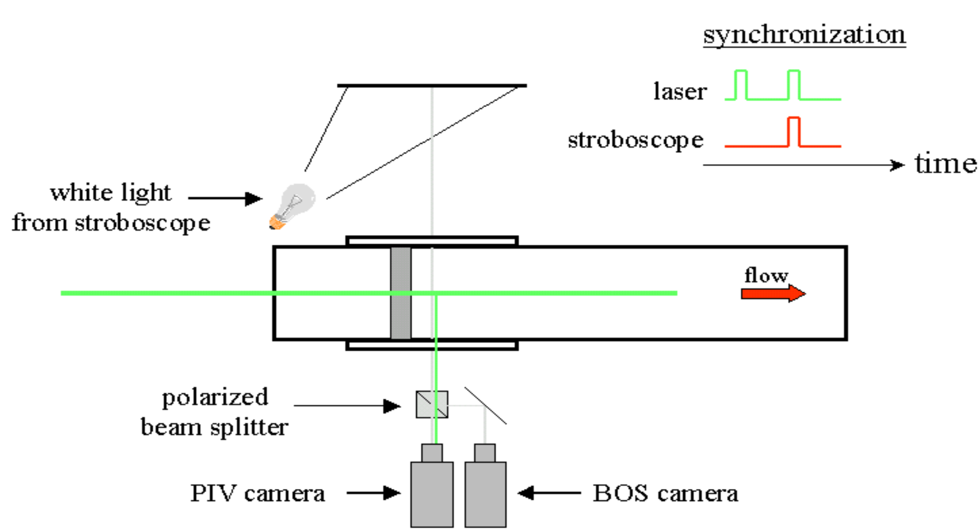

Fig.2.1: Test Set-up for PIV/BOS Combination

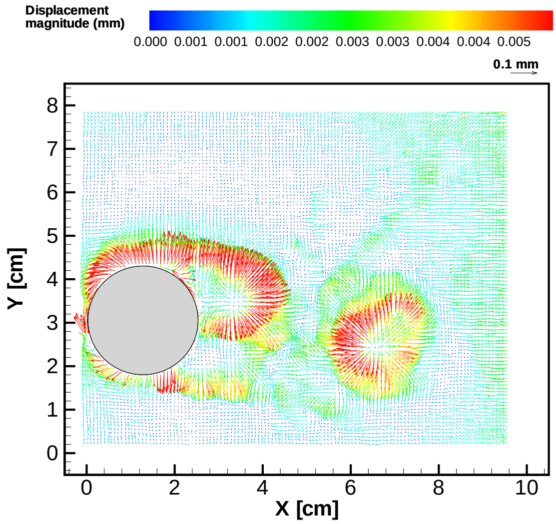

Fig.2.2 Displacement field proportional to density gradient, Re_d=211000 (BOS)

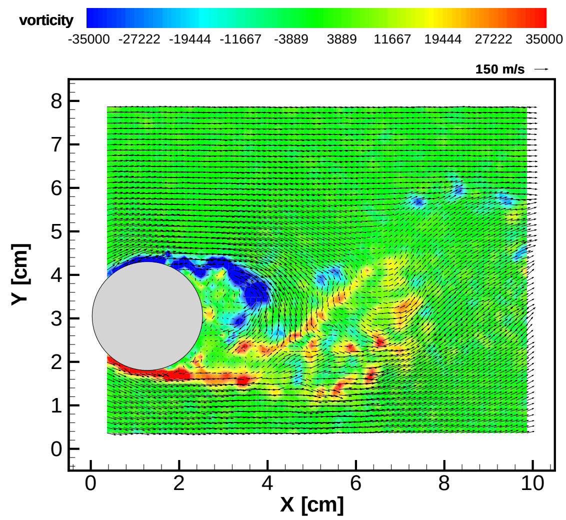

Fig.2.3 Velocity Field, Vorticity Contours (PIV)

cant influence of dissipation. Even if those assumptions are valid they limit the accuracy of the experimental results. Furthermore, the spatial-temporal derivatives of the pressure signal, which have to be computed in order to derive the induced velocities, amplify the noise and uncertainties of the data. The situation can be improved by simultaneous measurements of pressure, density, and velocity fields.

Fig.2.1 shows the setup needed in order to perform BOS and PIV measurements at the same time, which allows to get velocity and density information simultaneously. It is composed of two cameras, one used for PIV and the other for BOS. Both cameras have the same field of view and are looking through a polarized beam splitter, which blocks the light from the laser sheet for the BOS camera.

The PIV camera was focused on the laser light sheet plane, whereas the BOS camera was focused onto a background dot pattern generated by printing a single exposure PIV recording on a laser printer.

The stroboscope light was synchronized with the second pulse of the laser. The background of the second image is therefore brighter than the first, but the quality of the correlation data was not significantly reduced.

Fig.2.2 and **2.3** show respectively an example of BOS and PIV results for Re_d=211000 (Reynoldsnumber Re_d referred to cylinder diameter d) recorded at the same time. The vectors in Fig.2.2 are directly proportional to density gradient and are color coded according to the displacement magnitude.

Various phenomena can be clearly identified on both results, e.g. separation of the boundary layer, shear layer and vortex shedding.

It is obvious that the concentrations of vorticity as obtained from the PIV measurements (Fig.2.3) almost coincide with concentrations of pressure gradients seen in Fig.2.2.

Future effort is necessary to subtract from the data the physical information, i.e. the development and shedding of vortices from curved surfaces and their behavior in a compressible flow environment.

3. Dynamic Stall Experiment on Oscillating Airfoil (Part 2).

For the dynamic stall experiments the same wind tunnel facility has been used as already described in the previous section. But for the special purpose of dynamic stall investigations a new test section has been developed within the scope of the german project AROSYS (Active ROtor SYStems). This test section is now equipped with a servo motor to drive the model.

The dimensions of the new test section are:

Span: 0.1 m
Height: 0.35m

The model motion can either be sinusoidal:

$$\alpha=\alpha_o+\alpha_1 \sin(\omega*T)$$

with:

Mean incidence: $\alpha_{omax}=15^o$
Amplitude: $\alpha_{1max}=10^o$
Oscillation frequency: f_{max}=15 Hz

or the model can be moved in a ramp-type motion, i.e. with a constant angular velocity.

The motor rotates a circular plate which is plain with the back wall of the test section. The airfoil model is rigidly attached to this plate; a 4:1 gear is placed between motor and plate. To control the airfoils motion an angular pick-up is mounted directly on the moving plate. Eight pressure tabs, four at each side wall are located directly behind the wind tunnel nozzle to control the Mach number inside the test section. Inci-

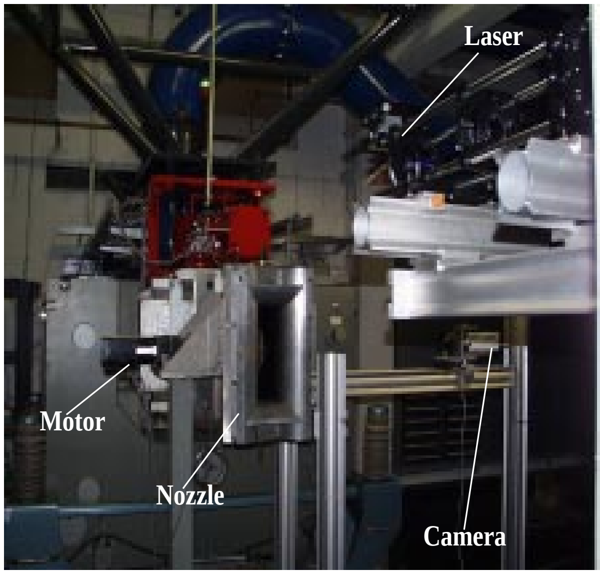

Fig.3.1 Test Overview

Fig.3.2 Observation Window

dence combinations and frequency selections can be made with the motor control unit.

Fig.3.1 shows an overview of the test setup. The wind tunnel used during these tests is of blow down type: the tunnel test section is connected to a vacuum chamber via a tube system. The flow is set into motion after opening the a remotely controlled valve.

The measuring time depends on the Mach number of the present test and is of the order of 30 - 45 seconds respectively. **Fig.3.2** shows the observation window including the airfoil model. The model is fixed to a circular plate opposite of the observation window and is suspended in a bearing inside the window glass. The axis of rotation is at quarter chord.

The Mach number of the tunnel is selected by a remotely controlled adjustment of a blocking rake which is installed downstream of the test section.

The PIV setup consisted of a Nd-Yag laser of 320 mJ per pulse. Two spherical and one cylindrical lens are needed to generate the light sheet. A 12 bits camera of 1280x1024 pixels resolution equipped with a 100 mm lens has been used. The laser is mounted in front of the test section. The laser light sheet illuminates the mid section of the model upper surface through the wind tunnel nozzle (see **Fig.3.1, Fig.3.3**).

This arrangement has the disadvantage that parts of the flow field are hidden inside the shadow of the model but minimize the direct reflections on the blade surface as it appears on the leading edge (see Fig.4.1). Due to the movement of the model the size of the shaded area is changing. In the data reduction procedure and in the experimental results these effects are taken into account (see section 4).

The parameters of the PIV processing are summarized in **Table 1.**

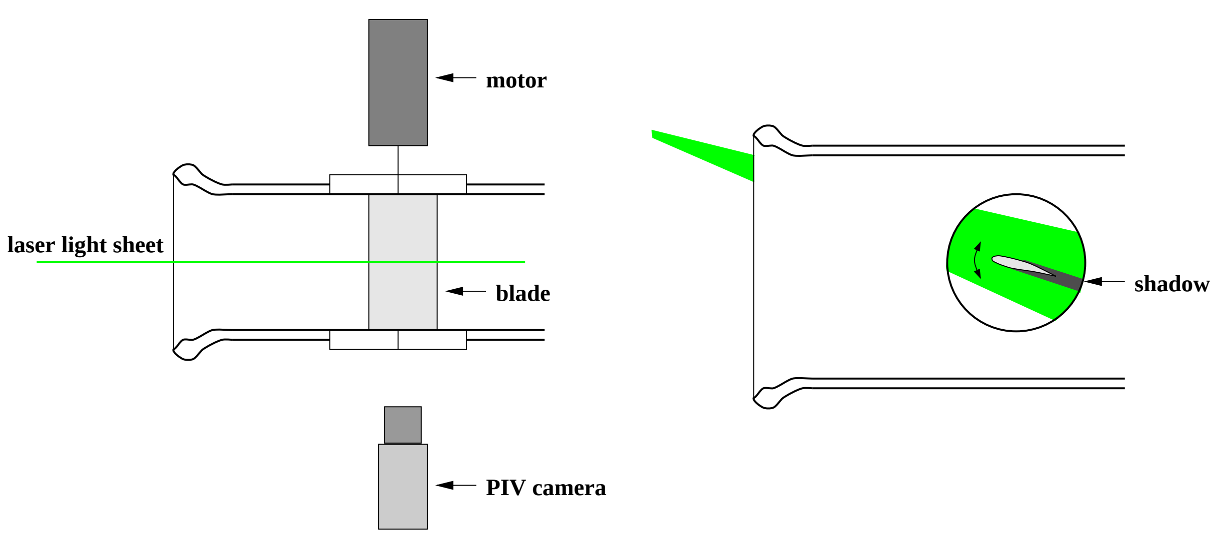

Fig.3.3: Sketch of PIV Test Setup

Table 1: PIV processing parameters

Image size	1280 x 1024 pixels
Calibration	153.44 pixels / cm
Time delay	4 µs for M=0.2 2 µs for M=0.3
Window size	24 x 24 pixels
Overlap	12 pixels
Number of vectors	102 x 81 vectors
Spatial resolution	0.082 cm

The shape of the blade as well as the shadow areas were masked for the processing and on the result presented. Most of the outliers are due to the reflection at the leading edge and have been removed. The removed data has been replaced by interpolated data from the adjacent flow field.

During the present dynamic stall tests the Mach number was varied between M=0.2 and M=0.3 (0.4). The corresponding measurement times were large enough to measure about 35 images with the PIV system. For the phase locked measurements of the laser system a trigger signal was given from the motor to the laser. Changing the time delay from the trigger signal the complete period of oscillation could be covered step by step.

Fig.3.4 shows measured incidence variations versus time. For comparison the (exact) sin-wave has also been indicated. Both the measured and the analytical curve show only very small deviations.

The servo motor realizes also the selected mean incidence and amplitude of oscillation. Under aerodynamic loads the amplitude is slightly reduced. The selected amplitude of 11^{o} in Fig. 3.4 is reduced to effectively 10.67^{o} at a Mach number of M=0.2. This value is stable over a sufficiently long time period.

Of importance is also the stability of the trigger signal produced by the motor control unit because this signal is used in order to synchronize together all PIV equipment.

4. Discussion of Results, Comparison of Experiment and Calculation

In the present section some selected experimental data will be compared with numerical results obtained with a 2D-time accurate Navier-Stokes code (RANS) which is described in detail in [8]. The structured grid is attached to the surface of the moving airfoil and to the fixed outer boundary respectively, i.e. the grid is deforming with respect to time during incidence variation. Grids are calculated in

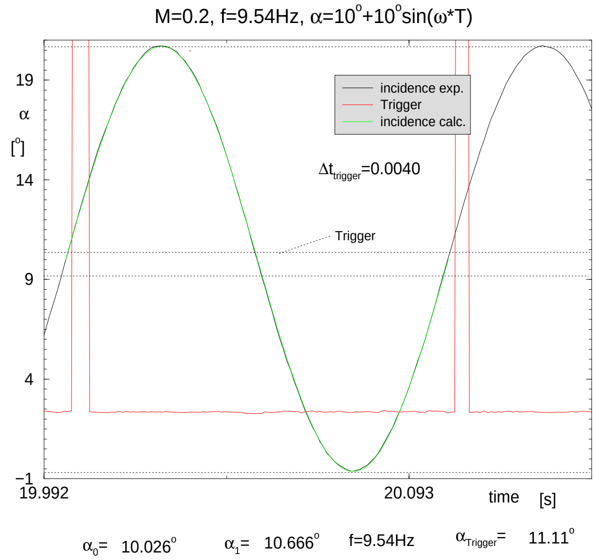

Fig.3.4: Measured and Calculated Incidence Variation and Trigger Location

advance for the maximum and minimum incidences respectively. Instantaneous grids are calculated during incidence variation by means of a linear interpolation procedure from the two extreme grids. The outer boundary is assumed 10 chord length away from the airfoil in all directions.

The calculations have been carried out on a 361x71 grid with the closest grid line $2x10^{-5}$ chord away from the airfoil surface.

The calculation has been done in three main steps:

1) Calculation of two grids at maximum and minimum incidence,

2) Calculation of steady start conditions at minimum incidence level. In the present case steady calculations have been carried out at $\alpha=0^{o}$ until a converged steady state result has been achieved.

3) Unsteady calculations are followed using the steady results as start condition.

The sinusoidal incidence variation is determined by

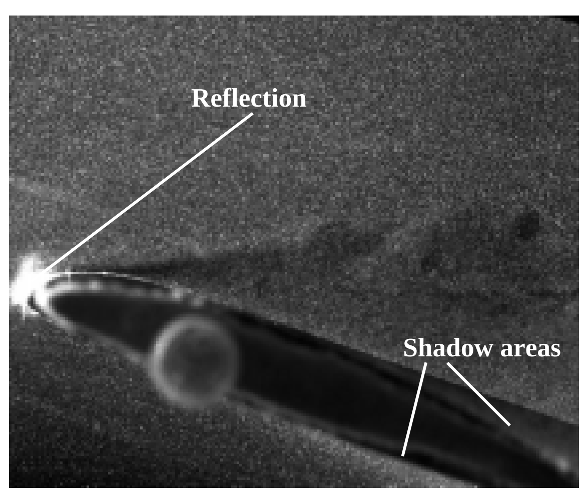

Fig.4.1: PIV test result, measuring area

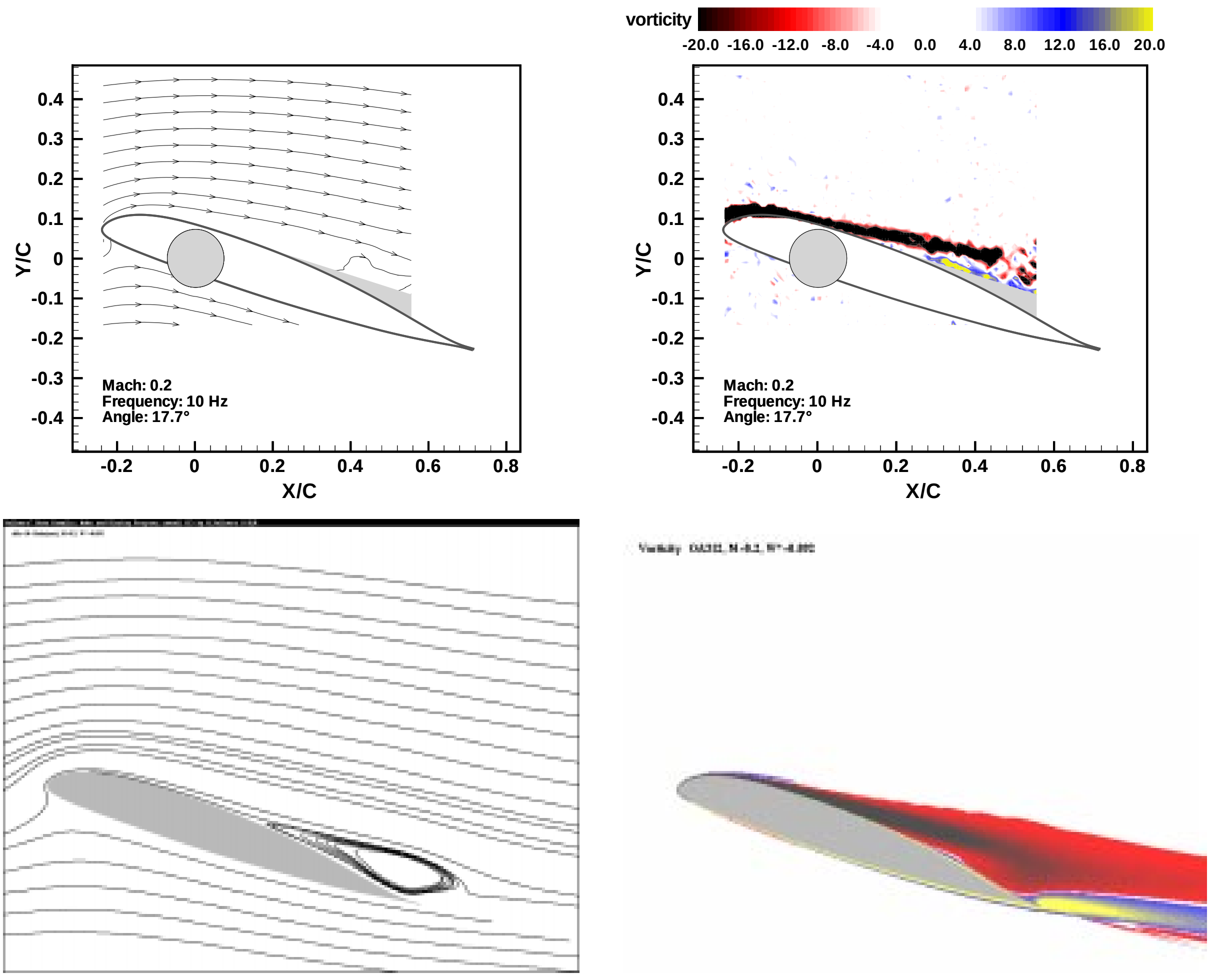

Fig. 4.2 Instantaneous Streamlines (left) and Vorticity Contours (right) from Experiment (upper figures) and from Calculation (lower figures). Incidence α=17.7^o up-stroke, M=0.2

$$\alpha=\alpha_0+\alpha_1 \sin(\omega^* T) \quad \text{(eq.1)}$$

with α_o as the mean incidence and α_1 as the amplitude of oscillation. ω^* is the reduced frequency defined as

$$\omega^*=2\pi f\, c/ U_\infty \quad \text{(eq.2)}$$

In the experiments as well as in the calculations the mean incidence and the amplitude were set to 10^o.

The incidence variation is therefore started at the minimum incidence (α=0^o) and continues to the maximum incidence at α=20^o (up-stroke region). It follows the down-stroke from α=20^o back to α=0^o. This first cycle is followed by at least one additional cycle until a converged periodic result (using force- and moment hysteresis loops as indicator) is achieved.

The number of time-steps per cycle is highly dependent on the value of the maximum Courant number which is proportional to the ratio of the time-step and the smallest grid cell. The Courant number has to be kept below about 1000 in the present code which is using an Approximate Factorization Implicit procedure of Beam and Warming type, [9].

In the present calculations the number of time-steps per cycle was set to 6x10^4. For the calculation the DLR NEC SX-5/16Be Supercomputer has been used for all calculations.

Results from the numerical calculations are available as:

- Lift-, drag- and pitching moment versus incidence (hysteresis loops) or versus time,
- chord wise pressure- and skin friction distributions for selected time steps
- field data, i.e velocity, pressure, density, Mach number, vorticity for selected time-steps.

The latter values are prepared to be used for visualization in video movie sequences.

In the experiment the instantaneous velocity vectors are measured with the Particle Image Velocimetry system. The measurements are done in a phase locked manner, i.e the phase delay from a trigger signal of the servo motor is selected. At each phase about 30 single pictures are taken. About 35 phases are measured to cover the complete cycle. The phases are concentrated in the region where the important

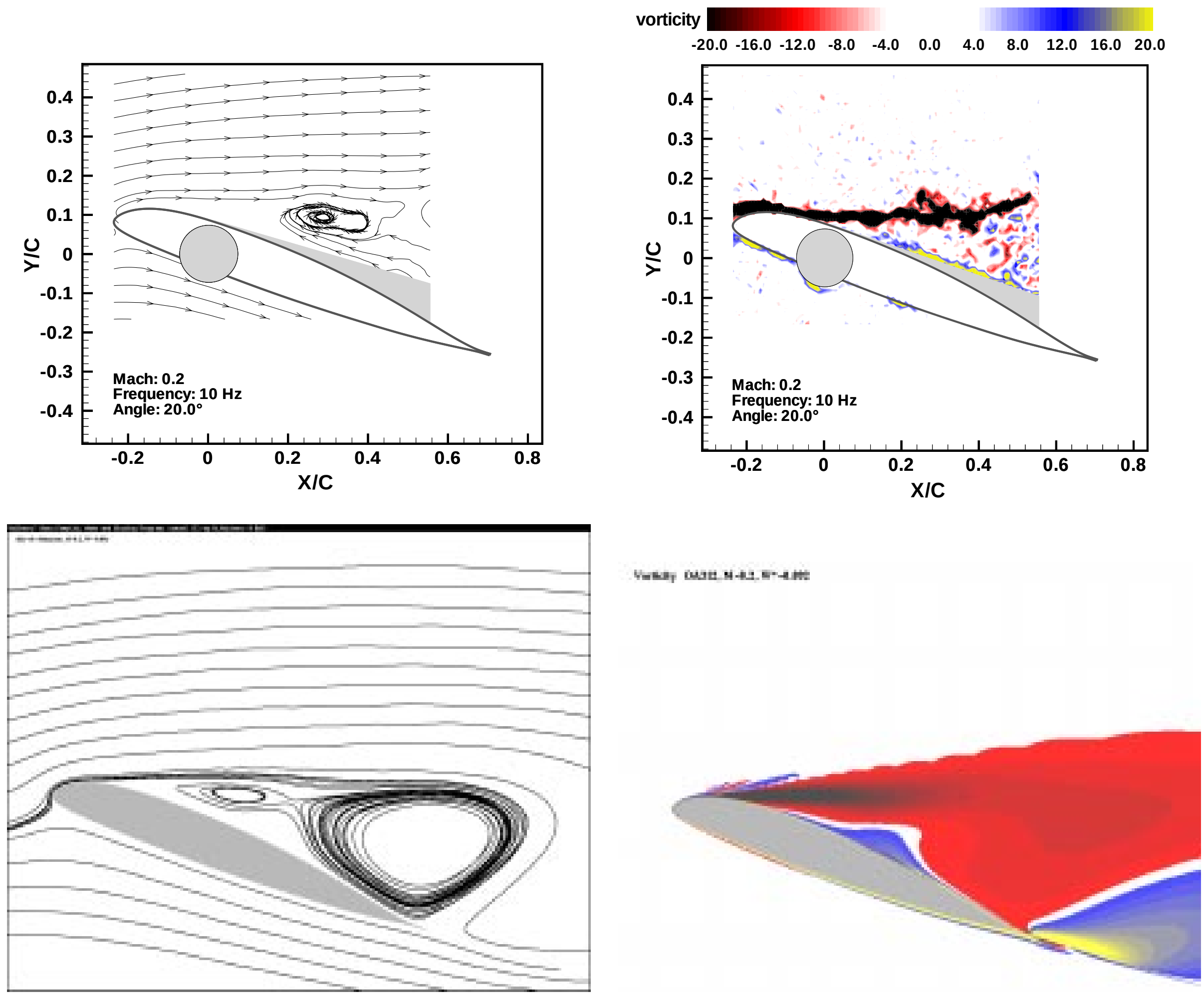

Fig. 4.3 Instantaneous Streamlines (left) and Vorticity Contours (right) from Experiment (upper figures) and from Calculation (lower figures). Incidence α=20.0^o down-stroke, M=0.2

flow events are to be expected. These regions are the up-stroke region between the mean incidence and the maximum incidence, as well as the high incidence part of the down-stroke region respectively.

The velocity vector fields are post processed to get the vorticity fields (differentiation) as well as the instantaneous streamlines (integration). These quantities are also available from the numerical calculation and therefore are ready for direct comparisons.

Fig. 4.1 shows the distribution of seeding material over the observation area which is concentrated over most part of the airfoil upper surface including the leading edge. A problem was the light spot at the leading edge of the airfoil indicated in Fig. 4.1. This spot was caused from reflections of the laser light sheet from the model surface. The reflection caused some losses of information in this area.

Another problem was caused by the special arrangement of the laser light sheet through the wind tunnel nozzle (see Fig.3.1). Dependent on the instantaneous position of the moving airfoil model some parts of the flow inside the observation area were covered by shadows (indicated in Fig.4.1).

Results for M=0.2.

Figs 4.2 and 4.3 show a selection of numerical and experimental results for two instantaneous incidences:

Fig.4.2: M=0.2, α= 17.7^o up-stroke

Fig.4.3: M=0.2, α=20.0^o beginning of down-stroke

The upper figures show the instantaneous streamlines (left) and vorticity distribution (right) of the experiment. The lower two figures show the corresponding results from the numerical calculations.

It is obvious in all figures that a strong separation of the flow has not yet been started although the incidence is already nearly 18^o. Due to the special airfoil shape which has a pre-drooping device the flow starts to separate from the trailing edge. This is clearly visible in all figures. The streamlines of both experiment and calculation show a recirculation zone at the trailing edge upper surface. The experimental figures are selected from the set of 30 PIV pictures as mentioned before. The vorticity distribution from the experiment shows a lot of scatter which is to be ex-

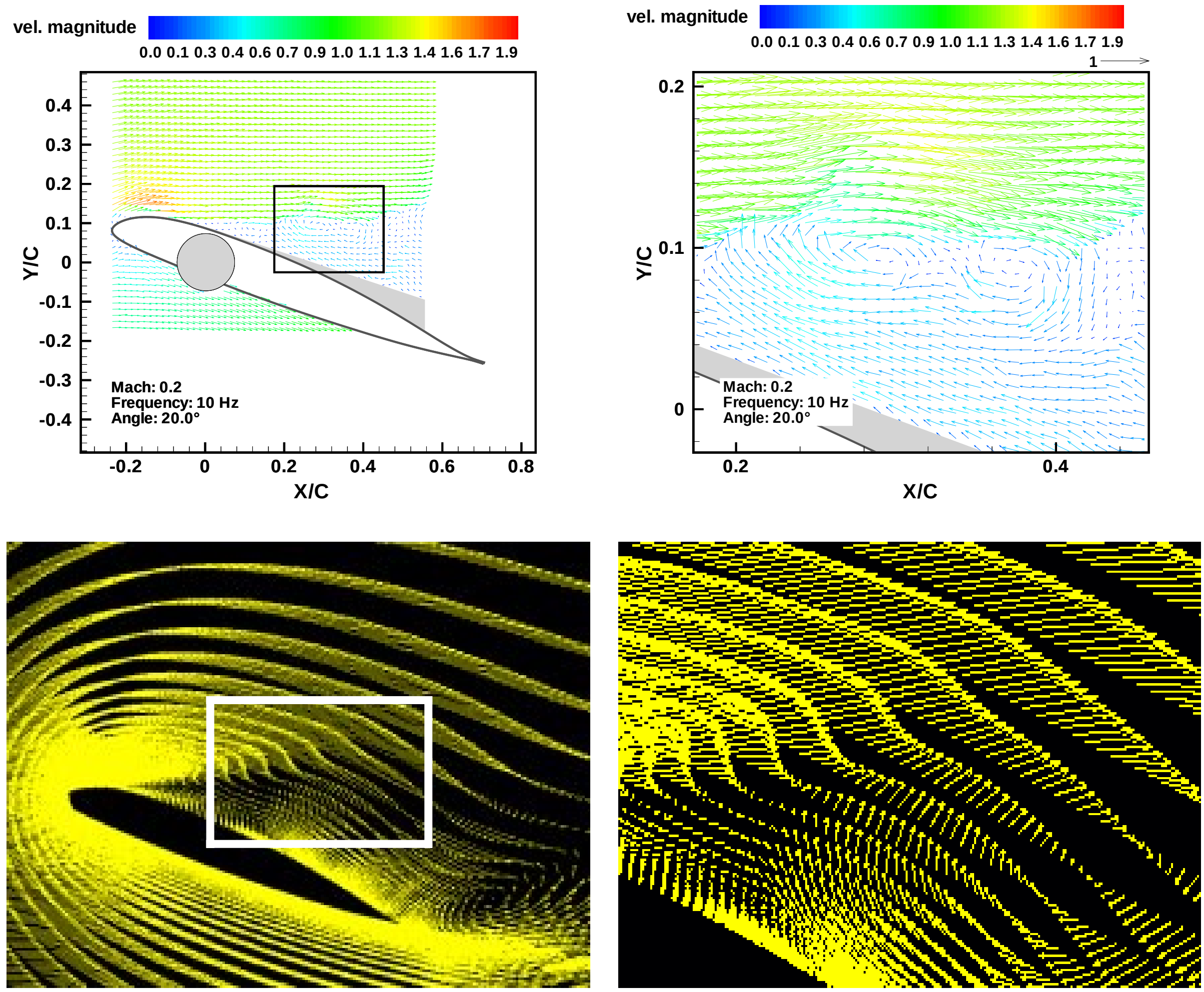

Fig. 4.4: Velocity vector fields at maximum incidence, left figures: total observation field, right figures: details of the flow field with double vortex system, α=20^o, M=0.2

pected due to influences of turbulence eddies inside this flow regime. At the leading edge the vorticity layer is too thick which must be attributed to the reflection problems indicated in Fig.4.1.The calculated vorticity contours are completely smooth: turbulence is only represented by a turbulence model which does not allow the representation of turbulence structures. In the calculation it was further assumed that the flow is fully turbulent, i.e. no transition from laminar to turbulent flow has been taken into account.

Fig.4.3 shows the flow situation at the maximum incidence α=20^o when the airfoil starts its way down (down-stroke regime). The single figures are arranged in the same way as in Fig.4.2.

Now severe separation occurs with large recirculation zones and multi vortex systems. The larger zone as indicated in the calculation is cut off by the edge of the observation area in the experimental case. The vorticity distributions are now lifted from the airfoil surface close to the leading edge upper surface. Again the increased thickness of the vorticity layer at the leading edge must be attributed to reflection effects. In color coded version the vorticity contours show in black to red: clockwise rotating vorticity and in yellow to blue: counter clockwise rotating vorticity respectively. The color coding was chosen to be equal in both experimental and numerical cases. It can be seen in both cases that a layer of counter rotating vorticity is located below the clock wise rotating vorticity. This „negative“ vorticity is created at the airfoil trailing edge where reversed flow is developing and moving up stream all the way towards the vicinity of the leading edge. Unfortunately the shadows along the airfoil upper surface hide these quite important effects in the experimental result. But in the calculation the reversed flow area is clearly visible.

Figs.4.4 show velocity vectors as measured by PIV (upper figures) and calculated (lower figures). A part of the flow field is selected and enlarged to show the detailed structure of the flow at the high incidence of α=20^o.

In both experimental and numerical data a pair of

vortices can be detected from the plots. In the experimental case the vortex centers are close together The numerical data show also two vortices but in larger distance. In all cases these vortices are clockwise rotating.
A further important feature of the dynamic stall process is the development of hysteresis effects, i.e. the flow behavior during the up-stroke motion differs considerably from the flow at the same incidence during the down-stroke motion. This behavior can clearly be detected from the experimental as well as from the numerical data (not shown).
It has already been mentioned that about 30 pictures have been made for one specific phase of the oscillation cycle. If the different pictures are compared it is obvious that considerable differences may occur from picture to picture indicating that the flow behaves very sensitive perhaps due to flow turbulence effects. For a better physical understanding of the flow fields it is preferable to use single picture information rather than to make averages over the total number of pictures. The latter procedure has been done in the present data reduction procedures and the results looked not very promising.
The reason is that the single pictures show details of vortex structures (see Fig.4.4) but these effects move from one picture to the next. Making averages the effects are completely smeared and a physical interpretation of the results is no longer possible.
All pictures with experimental data are therefore based on single picture information.

Results for M=0.3.
Figs.4.5 show results for the higher Mach number M=0.3. These figures are directly comparable with Figs. 4.2: the results are obtained at the same incidence of $\alpha=17.7^{o}$ up stroke. The oscillation frequency of the model is f=10Hz. Due to the higher Mach number the reduced frequency ω* as the dimensionless parameter characterizing the unsteadiness of the problem is reduced to ω*=0.061 compared to ω*=0.092 in the M=0.2 case (see Equation (2)). The effect due to this reduction is that the dynamic stall process is started already at a smaller incidence within the oscillatory loop. It can be detected from Figs.4.5 that compared to Figs. 4.2 the process of vortex development is already in a later stage. The

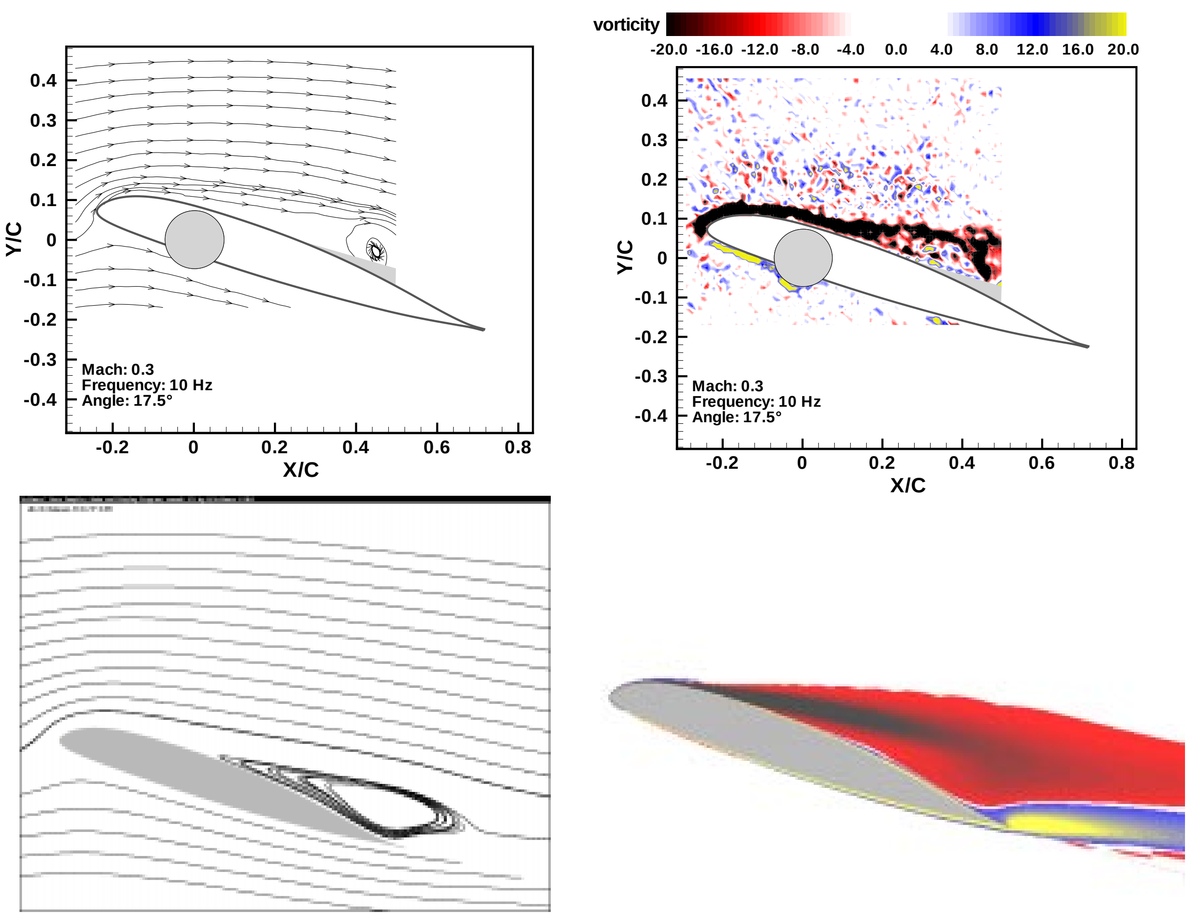

Fig. 4.5: Instantaneous Streamlines (left) and Vorticity Contours (right) from Experiment (upper figures) and from Calculation (lower figures). Incidence $\alpha=17.7^{o}$ down-stroke, M=0.3

effect on the calculated force- and moment hysteresis loops (not shown) are as follows: The maximum lift is reduced, drag rise and moment stall start earlier.

The second parameter involved i.e. the compressibility to a higher Mach number does play only a minor role: The large supersonic bubble as shown in Fig.2 on the NACA 23012 airfoil is not visible in the present case of a modern helicopter airfoil. The calculation has shown only a very small supersonic area at the airfoil leading edge which seems to have no larger effect on the dynamic stall process.

5. Conclusion

For the investigation of the unsteady flow on rotor airfoils new nonintrusive measuring techniques as the Particle Image Velocimetry (PIV) and a new method, the Background Oriented Schlieren (BOS) have first been applied in a simultaneous mode. The aim is to measure both the instantaneous velocity and density fields respectively and get more detailed insight into the complex flows involved.

The application for the flow about a circular cylinder has shown the feasibility of combining both measuring techniques.

The problem of more practical interest, i.e. the dynamic stall problem has been investigated next in a new wind tunnel test section equipped with a driving motor to oscillate the model. Here in a first step the Particle Image Velocimetry has been applied separately. In future investigations the combination of both PIV and BOS will be realized also for oscillating models.

The experimental data obtained during these tests show the main features of the dynamic stall process: development, growth and shedding of the dynamic stall vortex. These data are in good comparison with corresponding numerical results obtained with a time-accurate 2D-NS-code. It has been found that the development, growth and shedding of the dynamic stall vortex takes place in a very small time window of only a few incidence degrees. To catch the most important events of this process a sufficient number of PIV-sequences must be taken during this part of the loop. The numerical results may help as important information for this effort.

A problem of the PIV recordings taken for one phase was a considerable scatter in the data. This scatter makes the application of averaging procedures a formidable task. In the present paper the experimental data have been selected from a number of sequences as single pictures. These data include the turbulence content of the flow which is not included in the numerical data.

Acknowledgment:

The present investigations have been carried out within the DLR „Leitkonzept“ AROSYS (Active Rotor Systems). The support from this project is very much appreciated.

6. References

[1] McCroskey,W.J., "The phenomenon of dynamic stall", NASA TM 81264, 1981.

[2] Carr,L.W., McCroskey, W.J., "A review of recent advances in computational and experimental analysis of dynamic stall", Proc. IUTAM symposium on Fluid Dynamics of High Angle of Attack, Tokyo, Japan., 1992.

[3] Geissler, W., Raffel, M., "Dynamic Stall Control by Airfoil Deformation", Nineteenth European Rotorcraft Forum, Sept. 14-16, 1993, Cernobbio (Como), Italy, Proceedings pp. C2-1 C2-13

[4] Geissler,W.,Vollmers,H. “Unsteady Separated Flows on Rotor-Airfoils -Analysis and Visualization of Numerical Data-” Eighteenth European Rotorcraft Forum, Sept.15-18, 1992, Avignon, France. Proceedings pp. 79.1-79.12

[5] Carr,L.W., Chandrasekhara,M.S., "Compressibility Effects on Dynamic Stall", Prog. Aerospace Sci. Vol 32, pp. 523-573, 1996

[6] Raffel, M., Willert, C., Kompenhans, J., “Particle Image Velocimetry - A Practical Guide”, Springler, 1998

[7] Richard, H., Rein, M., Meier, G.E.A., Kompenhans, J., Raffel, M., “On the applicability of a background oriented schlieren (BOS) method”, Tenth Int. Symp. on Appl. of Laser Techniques to Fluid Mechanics, Lisbon, Portugal, July 2000.

[8] Geissler,W. “Verfahren in der instationären Aerodynamik (Methods in Unsteady Aerodynamics)” in german, *DLR-FB 93-21 (1993) also in:*
DLR-FB 92-03 (1992)
516 pages,227 figures,183 references

[9] Beam,R.,Warming,R.F.,“An Implicit Factored Scheme for the Compressible Navier-Stokes Equations,“
AIAA J.,Vol.16,No.4 (April 1978).